Adsorption of Asphaltenes in Porous Media under Flow Conditions

ARTICLE *in* ENERGY & FUELS · OCTOBER 2010

Impact Factor: 2.79 · DOI: 10.1021/ef100881k

3 AUTHORS, INCLUDING:

Soheil Saraji
University of Wyoming
15 PUBLICATIONS **97** CITATIONS
SEE PROFILE

Lamia Goual
University of Wyoming
32 PUBLICATIONS **554** CITATIONS
SEE PROFILE

Energy Fuels **2010,** *24,* 6009–6017 · DOI:10.1021/ef100881k
Published on Web 11/01/2010

energy&fuels
article

Adsorption of Asphaltenes in Porous Media under Flow Conditions

Soheil Saraji, Lamia Goual,* and Mohammad Piri

Department of Chemical and Petroleum Engineering, University of Wyoming, Department 3295, 1000 East University Avenue, Laramie, Wyoming 82071, United States

Received July 9, 2010. Revised Manuscript Received September 25, 2010

Asphaltene adsorption on minerals induces wettability alteration in porous media, which, in turn, affects capillary pressure, relative permeability, and residual oil saturations. The majority of existing work addresses the adsorption of asphaltenes on minerals under static conditions, where adsorption isotherms are measured and modeled. Very little work currently exists on the adsorption kinetics of asphaltenes under dynamic conditions, which are more relevant to laboratory-scale experiments, specifically those involving dynamic wettability alteration of minerals. In this study, we propose to investigate the dynamic adsorption of different asphaltenes on various minerals using UV−vis spectroscopy. The experimental setup consists of a core holder containing crushed minerals with comparable mesh size. Asphaltene solutions in toluene are then flown though the mineral pack with a constant flow rate, and their concentrations are recorded with time at the outlet. Preliminary results indicate that adsorption is largely controlled by the type of mineral rather than the asphaltene itself. The highest adsorption amounts per unit area are found on calcite. Furthermore, the effect of several parameters, such as concentration, asphaltene composition, and flow rate, are considered. The theory of activated adsorption/desorption (TAAD) approach (Rudzinski, W.; Plazinski, W. *J. Phys. Chem. C* 2007, *111*, 15100−15110) is incorporated into the convection-dispersion transport equation to model the flow of asphaltenes inside the porous medium. The resulting equation is then solved numerically using Barakat−Clark finite difference technique (Satter, A.; Shum, Y.; Adams, W.; Davis, L. *SPE J.* 1980, *20*, 129−138). We find that kinetics and not equilibrium governs asphaltene adsorption in porous media. Levenberg−Marquardt's optimization algorithm is used to derive kinetic parameters, such as Γ_m, k_a, and k_d. Once these concentration-independent parameters are found, the model is able to predict with reasonable accuracy the effect of concentration on asphaltene adsorption in porous media.

Introduction

Flow and distribution of fluids in porous media are largely controlled by fluid−fluid and rock−fluid interactions. In laboratory studies involving wettability alteration, the interaction of petroleum asphaltenes and mineral surfaces is often used to alter the wettability of cores toward more oil-wet conditions. Recently, dynamic aging of rock core samples by continuous flooding of crude oils was proposed for more effective and uniform wettability alteration.[3,4]

There is a large body of literature that deals with the adsorption of asphaltenes on various rock minerals, including clays. Most of these works are concerned with the measurement and modeling of adsorption isotherms on crushed minerals under static conditions.[5−14] Only a few studies currently exist on the kinetics of asphaltene adsorption under static conditions.[15,16] Both irreversible adsorption[9,17,18] and reversible adsorption[19] have been suggested in the past. Acevedo et al.[17] observed that, by increasing the asphaltene concentration, the rate of adsorption decreases and the adsorption capacity increases. The authors claimed that this behavior is the result of different adsorption kinetics for aggregates as compared to monomers. Lopez-Linares et al.[18] found that the rate of asphaltene adsorption on different minerals increases

*To whom correspondence should be addressed. E-mail: lgoual@uwyo.edu.

(1) Rudzinski, W.; Plazinski, W. *J. Phys. Chem. C* **2007**, *111*, 15100–15110.
(2) Satter, A.; Shum, Y.; Adams, W.; Davis, L. *SPE J.* **1980**, *20*, 129–138.
(3) Graue, A.; E. Aspenes, R. M. J. R.; Bognø, T. *J. Pet. Sci. Eng.* **2002**, *33*, 3–17.
(4) Fernø, M. A.; Torsvik, M.; Haugland, S.; Graue, A. *Energy Fuels* **2010**, *24*, 3950–3958.
(5) Dubey, S.; Waxman, M. *SPE Res. Eng. J.* **1991**, *6*, 389–395.
(6) González, G.; Travalloni-Louvisse, A. *SPE Prod. Facil.* **1993**, *8*, 91–96.
(7) Pernyeszi, T.; Patzkó, A.; Berkesi, O.; Dékány, I. *Colloid Surf., A* **1998**, *137*, 373–384.
(8) Acevedo, S.; Castillo, J.; Fernández, A.; Goncalvez, S.; Ranaudo, M. *Energy Fuels* **1998**, *12*, 386–390.
(9) Acevedo, S.; Ranaudo, M.; García, C.; Castillo, J.; Fernández, A.; Caetano, M.; Goncalvez, S. *Colloid Surf., A* **2000**, *166*, 145–152.
(10) Marczewski, A.; Szymula, M. *Colloid Surf., A* **2002**, *208*, 259–266.
(11) Dudasova, D.; Simon, S.; Hemmingsen, P.; Sjoblom, J. *Colloid Surf., A* **2008**, *317*, 1–9.
(12) Jouault, N.; Corvis, Y.; Cousin, F.; Jestin, J.; Barre, L. *Langmuir* **2009**, *25*, 3991–3998.
(13) de la Cruz, J. M.; Castellanos-Ramírez, I.; Ortiz-Tapiac, A.; Buenrostro-González, E.; Durán-Valenciad, C.; López-Ramírez, S. *Colloid Surf., A* **2009**, *340*, 149–154.
(14) Xing, C.; Hilts, R. W.; Shaw, J. M. *Energy Fuels* **2010**, *24*, 2500–2513.
(15) Dudasova, D.; Silset, A.; Sjoblom, J. *J. Dispersion Sci. Technol.* **2008**, *29*, 139–146.
(16) Abudu, A.; Goual, L. *Energy Fuels* **2009**, *23*, 1237–1248.
(17) Acevedo, S.; Ranaudo, M.; García, C.; Castillo, J.; Fernández, A. *Energy Fuels* **2003**, *17*, 257–261.
(18) Lopez-Linares, F.; Carbognani, L.; Sosa-Stull, C.; Pereira-Almao, P.; Spencer, R. *Energy Fuels* **2009**, *23*, 1901–1908.
(19) Syunyaev, R.; Balabin, R.; Akhatov, I.; Safieva, J. *Energy Fuels* **2009**, *23*, 1230–1236.

Table 1. Properties of Selected Asphaltenes and Crude Oils

sample	$\rho^{20\ °C}$ (g/mL)	C (%)	H (%)	N (%)	O (%)	S (%)	H/C	ASPH (wt %)	TAN (mg of KOH/g)	TBN (mg of KOH/g)	TBN/TAN
Gibbs	0.905	84.74	7.52	1.10	1.12	5.68	1.06	10.23	0.146	2.466	16.9
Minnelusa	0.871	86.69	6.65	0.83	1.36	4.51	0.92	3.29	0.110	0.955	8.6
Canadian	0.943	81.29	8.18	1.10	1.41	8.28	1.21	14.04	1.140	2.797	2.5

Table 2. Properties of Selected Minerals

sample	source	rock density (g/mL)	BET surface area (m_2/g)	cumulative pore volume (mL/g)	average pore diameter (Å)
calcite	Chihuahua, New Mexico	2.71	0.0995	0.001221	201.40
quartz	Hot Spring, Arkansas	2.65	0.2136	0.001126	103.08
dolomite	New Jersey	2.70	0.2844	0.001696	130.44

with increasing aromaticity and nitrogen content and decreasing molecular size. Syunyaev et al.[19] reported that the chemical composition and structural parameters of the mineral surface are the main factors that control the adsorption process. In addition, they found different rate constants for different particle sizes of the same material. This phenomenon was explained by higher contact points per unit volume for finer grain fractions, which act as nucleation sites for adsorption.

Very little work currently exists on the adsorption kinetics of asphaltenes under flow conditions. Piro et al.[20] used a sand pack of crushed dolomite and asphaltene-in-toluene solution to investigate their dynamic adsorption under different flow rates. The authors found that the amounts of adsorbed asphaltenes are rate-dependent. The continuous adsorption with time observed in their study is possibly due to uncertainties in the estimation of initial concentrations. More recently, the adsorption of asphaltenes on minerals was studied under flow conditions using a quartz crystal microbalance with dissipation monitoring (QCM-D).[15,16] It was shown that the solubility of asphaltenes in the liquid phase affects the mechanical properties of the adsorbed film[16] and that the amount of adsorbed asphaltenes can be correlated to their nitrogen content.[15] The advantage of QCM-D is its high mass sensitivity; however, the type of mineral coating on QCM-D crystals is usually very limited.

Adsorption under static conditions can be governed by two processes: kinetics and equilibrium. In the kinetic process, solutes exhibit adsorption that is significantly rate-controlled or time-dependent, whereas in the equilibrium process, adsorption is relatively instantaneous because of strong solute−adsorbent interactions and only the final state of a system is measured.[21] In processes involving flow through porous media convection−dispersion effects are considered and it is the relative rate of adsorptive and convective−dispersive mass transfer that determines whether adsorption/desorption kinetics or adsorption equilibrium governs the adsorption process.[22] This phenomenon has been investigated in groundwater contaminant transport and chemical flooding in oil reservoirs for four decades.[2,22−24] Either adsorption equilibrium or kinetic equations are incorporated into the convection−dispersion−adsorption model to simulate the experimental data.

In this study, a series of dynamic experiments on mineral packs were conducted to investigate adsorption of asphaltenes on various minerals under flow conditions. Our goal is to understand rock−asphaltene interactions when flow is involved. Experimental data were then modeled numerically by a convection−dispersion−adsorption solute transport equation to derive adsorption kinetic parameters and possible correlations with fluid and rock properties.[1,21]

Materials and Methods

Crude Oils and Asphaltenes. Three crude oils were used in this work. Gibbs and Minnelusa oils are from Wyoming (U.S.A.), while Canadian oil is from Alberta (Canada). The oils were first centrifuged at 3000 rpm to remove any impurities, such as mineral fines, and then filtered with 2 μm metal inline filter prior to asphaltene separation. Asphaltenes were precipitated from crude oils using *n*-pentane (98% pure, EMD Chemicals, Inc.) according to a procedure described elsewhere.[25] The extracted asphaltenes were stored in a desiccator for at most 7 days before use. Asphaltene solutions were then prepared by dissolving asphaltenes in dry toluene (HPLC grade, Fisher Scientific) and stirring the solution for 60 min. Dry toluene was obtained from distillation of toluene with a rotary evaporator to remove any traces of water. The solutions were usually stored for at least 12 h to reach equilibrium. Some properties of the crudes and separated asphaltenes are listed in Table 1. The densities were measured using a DMA45 density meter (Anton-Paar, Ashland, VA). The total acid number (TAN) and total base number (TBN) of these oils were measured at least three times by a Metrohm 808 titrando titrator. The elemental analysis was performed by Huffman Laboratory in Golden, CO.

Minerals. All minerals were purchased from Ward's Natural Science as rock pieces. The rocks were crushed in three steps in a rock-crushing lab and then sieved. The crushed rocks were then washed with distilled water to remove any dust and dried in an oven at 110 °C. The rock particle sizes between 74 and 150 μm (100−200 mesh sizes) were used in all of our experiments. The Barret, Joyner, and Halenda (BJH) method[26] was applied to the crushed minerals to determine their physical properties (see Table 2). An appropriate amount of minerals was dried in an oven at 110 °C, a day prior to starting the experiment, and then stored in a desiccator a few hours before use.

Experimental Setup and Procedure. Dynamic adsorption experiments were performed using a core flooding setup depicted in Figure 1. The setup consisted of a dual-cylinder Teledyne Isco pump model 260D to provide a constant continuous flow rate, a 2 L stainless-steel accumulator, an aluminum sand-pack holder (2.53 cm inner diameter and 10.4 cm length) with fixed and adjustable end caps, and a double-beam UV−vis spectrophotometer

(20) Piro, G.; Canonico, L.; Galbariggi, G.; Bertero, L.; Carniani, C. *SPE Prod. Facil.* **1996**, *11*, 156–160.
(21) Azizian, S. *J. Colloid Interface Sci.* **2004**, *276*, 47–52.
(22) Mannhardt, K.; Nasr-El-Din, H. *In Situ* **1994**, *18*, 277–345.
(23) Gupta, S.; Greenkorn, R. *Water Resour. Res.* **1974**, *10*, 839–846.
(24) Grattoni, C.; Dawe, R.; Bidner, M. *Adv. Water Resour.* **1993**, *16*, 127–135.
(25) Goual, L.; Firoozabadi, A. *AIChE J.* **2002**, *48*, 2646–2663.
(26) Barrett, E.; Joyner, L.; Halenda, P. *J. Am. Chem. Soc.* **1951**, *73*, 373–380.

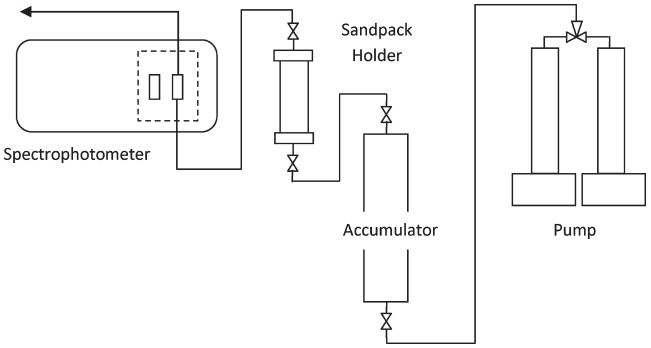

Figure 1. Schematic of the experimental setup.

(Cary 4000, Varian, Inc.) to measure concentrations. First, the sieved, washed, and dried mineral (74−150 μm) was packed inside the sand-pack holder. The weight and length of the sand pack were then recorded. This information was used to calculate porosity. Next, the sand pack was vacuumed and saturated with pure distilled toluene. The outlet line and flow cell inside the spectrophotometer were also filled with pure toluene. Finally, the asphaltene solution, placed in an accumulator, was injected through the pack with a constant flow rate. Changes in the outlet concentration were recorded automatically by the spectrophotometer at a predefined frequency.

The spectrophotometer used in this study was slightly modified to accommodate a quartz flow cell (Starna Cells, Inc.) with a 4 mL nominal volume and 10 mm path length in the sample compartment. Having a flow cell allowed us to monitor concentrations automatically at the outlet in real time. Mixing effects or early breakthrough inside the flow cell might be of concern because they may affect the real concentration values. Therefore, a series of tests were conducted by providing a step change in concentration (500 mg/L versus pure toluene) at the inlet of the flow cell and monitoring absorbance values. The absorbance reached that of 500 mg/L solution in static measurements, with less than 4 mL at flow rate ranges used in this study. This observation shows that, at the specified flow rates, flow effects inside the flow cell do not have significant adverse effects.

To calibrate the spectrophotometer for each asphaltene sample, a stock asphaltene-in-toluene solution of 500 mg/L was prepared and diluted for making lower concentration solutions. Then, absorbance of each solution was measured in the 200−800 nm range. Usually, absorbance peak (~290 nm) readings are used for calibration at concentrations less than 100 mg/L.[10,27] However, for higher concentrations, the absorbance level at this point exceeds the output range of the instrument. For this reason, a higher wavelength is usually selected.[7,12,27] Here, 510 nm was selected as the calibration wavelength. It gives acceptable accuracy ($R^2 > 0.9999$) in the full concentration range (0−500 mg/L) of asphaltenes listed in Table 1. The calibration graphs for all asphaltenes are shown in Figure 2.

A concern in adsorption experiments using UV-vis spectroscopy is the selective adsorption of asphaltenes, which may alter the average composition of asphaltenes at the outlet and, hence, change the UV−vis spectra and introduce an error in concentration calculations.[27,28] To estimate the range of this error, the outlet solution was collected during experiment 2, filtered by 0.2 nm membrane filter to remove mineral fines, and then dried under the hood. The recovered asphaltenes were used to reconstruct the calibration graph. A comparison between the original and the outlet asphaltene calibration curves using a method proposed by Alboudwarej et al. shows less than 5% error in the concentration calculations.

(27) Alboudwarej, H.; Jakher, R.; Svrcek, W.; Yarranton, H. *Pet. Sci. Technol.* **2004**, *22*, 647–664.
(28) Ruiz-Morales, Y.; Wu, X.; Mullins, O. C. *Energy Fuels* **2007**, *21*, 944–952.

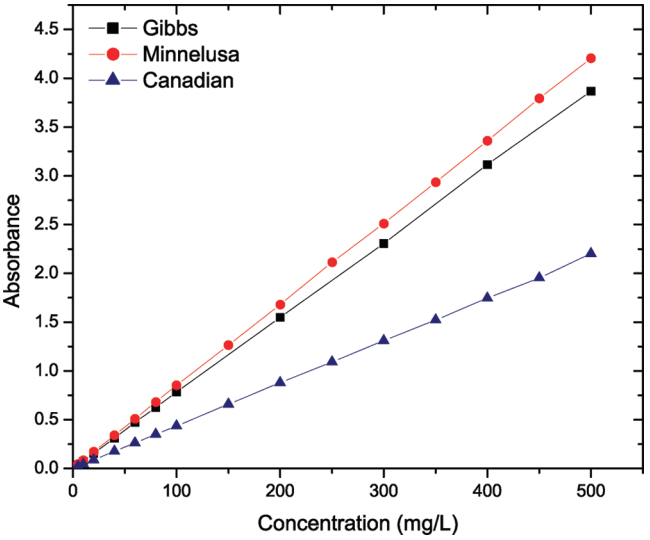

Figure 2. Absorbance−concentration calibration for asphaltenes.

Modeling. Adsorptive flow-through porous media are governed by the convection−dispersion−adsorption transport equation, which in one dimension has the form[2]

$$D\frac{\partial^2 C}{\partial x^2} - v\frac{\partial C}{\partial x} = \frac{\partial C}{\partial t} + \left(\frac{1-\phi}{\phi}\right)\rho_r\frac{\partial \Gamma}{\partial t} \quad (1)$$

where C is the solute concentration, Γ is the adsorbed mass of solute per unit mass of solid, x is the distance, t is the time, D is the dispersion coefficient, v is the interstitial velocity, ϕ is the porosity, and ρ_r is the mineral density.

Equation 1 is usually coupled with various adsorption kinetics equations and/or equilibrium adsorption models to model experimental data in different applications from groundwater contamination transport to surfactant and polymer flooding.[2,22−24] In this study, the theory of activated adsorption and desorption (TAAD) is used to model adsorption kinetics

$$\frac{\partial \Gamma}{\partial t} = k_a C(\Gamma_m - \Gamma) - k_d \Gamma \quad (2)$$

where k_a and k_d are concentration-independent adsorption and desorption constants and Γ_m is the maximum amount of adsorption.

Under certain conditions, eq 2 can be simplified to the well-known pseudo-first-order and pseudo-second-order kinetic equations.[21] At equilibrium ($\partial\Gamma/\partial t = 0$), eq 2 becomes the Langmuir adsorption isotherm

$$\Gamma = \frac{\Gamma_m K_L C}{1 + K_L C} \quad (3)$$

where

$$K_L = \frac{k_a}{k_d} \quad (4)$$

Langmuir adsorption is used here for modeling adsorption equilibrium. Equation 3 is differentiated with respect to time and used in eq 1 to obtain

$$D\frac{\partial^2 C}{\partial x^2} - v\frac{\partial C}{\partial x} = \left[1 + \frac{(1-\phi)\Gamma_m K_L \rho_r}{\phi(1+K_L C)^2}\right]\frac{\partial C}{\partial t} \quad (5)$$

To solve the kinetic equations (eqs 1 and 2) and equilibrium equation (eq 5) numerically, they were first converted into dimensionless forms. The dimensionless forms of these equations along with their boundary and initial conditions are listed in the

Appendix. Two separate Matlab programs were developed to numerically solve eqs A1 and A2 (see the Appendix) simultaneously for the kinetic case and eq A7 for the equilibrium case. For this purpose, the Barakat−Clark finite difference scheme was used to discretize the equations.[2] The values of spatial increment (ΔX_D) and time step (ΔT_D) used in this work were 0.005 and 0.0006, respectively. These values were obtained by optimizing the numerical results for the non-adsorption case ($N_{Ae} = N_A = N_v = N_k = 0$) compared to theoretical results provided by Coats and Smith.[29] In addition, a nonlinear least-squares optimization algorithm (Levenberg−Marquardt)[24,30] was used in combination with the numerical scheme to obtain either kinetic parameters of adsorption (Γ_m, k_a, and k_d) or Langmuir parameters (Γ_m and K_L) by fitting the experimental data.

Results and Discussion

Dispersion. To estimate the dispersion coefficient, D, in eq 1, a separate experiment was conducted with a non-adsorbing fluorescent dye called DFSB-C0 (Risk Reactor, Inc.). The dye was dissolved in pure distilled toluene at a concentration of 250 mg/L prior to injection. This solution is colorless in the visible range but has detectable absorbance in the ultraviolet wavelength range. The spectrophotometer calibration was performed at 300 nm, where there is a maximum separation between concentration curves. To check possible adsorption of the dye on quartz, a batch experiment was performed by adding 10 mL of dye in toluene solution to 1 g of quartz mineral. No adsorption was detected after 24 h. A quartz pack was then prepared, and a flow experiment was conducted at 0.5 mL/min flow rate. The measured concentration breakthrough curve, presented in Figure 3, was prepared by normalizing the outlet concentration to a constant injection concentration measured separately before the start of the experiment. The curve is symmetrical and crosses 1 pore volume at around 0.5 C/C_0 value, as expected.[29] Our transport model was then used to simulate the experimental data by considering no adsorption ($N_{Ae} = N_A = N_v = N_k = 0$). The resulting fit is shown in Figure 3 with an optimum dispersion coefficient of 2.109×10^{-4} cm^2/s.

Because all mineral packs used in this study have particle sizes in the range of 74−150 μm, the same dispersion coefficient is used for modeling all experiments performed at 0.5 mL/min flow rate. For other flow rates, a linear correlation between the dispersion coefficient and interstitial velocity was considered and dispersion values were estimated at the desired flow rate.[31] This correlation was used because our flow rates are in the range where the mechanical dispersion is dominant. Researchers have shown that the dispersion coefficient follows different behaviors at different ranges of the Peclet number.[32] At low Peclet numbers (<0.4), molecular diffusion is dominant, while at intermediate Peclet numbers (2−100), the effect of molecular diffusion diminishes significantly, leading to the dominance of mechanical mixing. In this regime, the dispersion coefficient increases linearly by increasing the Peclet number (interstitial velocity). At extremely high Peclet numbers (>10 000), there is no linear relation between D and velocity.[22,31] The size difference between the dye molecules and asphaltene nano-aggregates has, therefore, little impact here because the effect of the molecular diffusion is negligible in the flow regime that is relevant to our flow experiments.

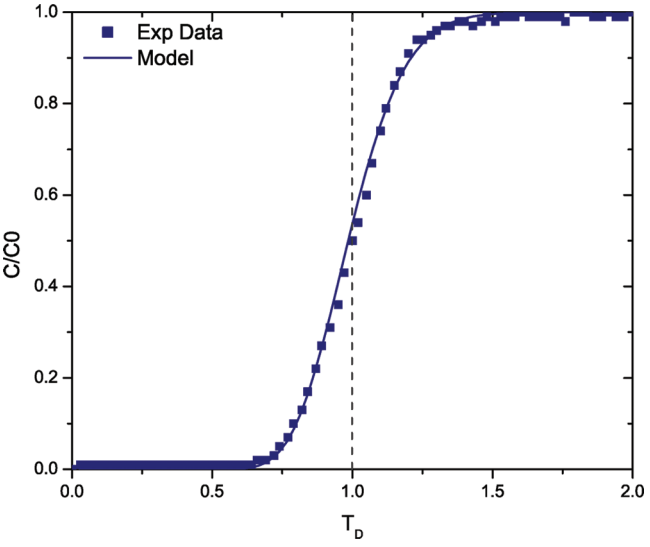

Figure 3. Concentration profile of the dye dispersion in porous media.

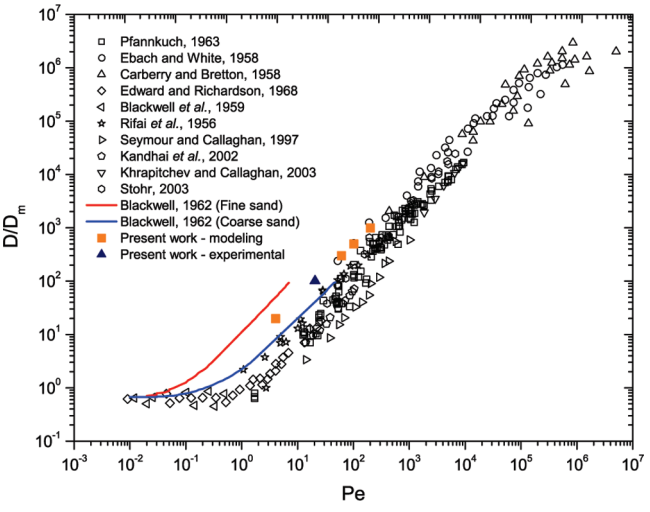

Figure 4. Dimensionless dispersion coefficients for various porous media at different hydrodynamic conditions.[33−34,46−54]

Figure 4 compares the experimentally obtained and estimated dispersion coefficients in this study along with values reported in the literature. Our values are in good agreement with those in the literature, particularly for unconsolidated porous media, such as those reported by Ebach and White[33] and Blackwell.[34] Furthermore, our measured and predicted dispersion values are located in the middle of Blackwell's proposed region. Grain sizes in our sand packs were in the 74−150 μm range, which is comparable to the medium-size sand category of Blackwell's study.

Adsorption. Table 3 presents the dynamic adsorption experiments performed with various minerals and asphaltenes. For each experiment, information related to the sand pack and the adsorbed amounts, obtained using material balance

(29) Coats, K.; Smith, B. *SPE J.* **1964**, *4*, 73–84.
(30) MathWorks. *Optimization Toolbox for Use with MATLAB User's Guide*; MathWorks, Inc.: Natick, MA, 2001.
(31) Perkins, T.; Johnston, O. *SPE J.* **1963**, *3*, 70–84.
(32) Bear, J. *Dynamics of Fluids in Porous Media*; Dover Publications: Mineola, NY, 1988.
(33) Ebach, E.; White, R. *AIChE J.* **1958**, *4*, 161–169.
(34) Blackwell, R. *SPE J.* **1962**, *2*, 1–8.

Table 3. Adsorption Tests

test	asphaltene	C_0 (mg/L)	q (mL/min)	ϕ (%)	rock weight (g)	holder length (cm)	Γ_{exp} (mg/m^2)
				Calcite			
1	Gibbs	503	0.1	44.26	64.8	8.57	3.48
2	Gibbs	503	0.5	43.52	66.6	8.70	3.63
3	Gibbs	504	1.5	43.81	64.8	8.50	3.29
4	Gibbs	509	2.5	44.03	66.0	8.69	2.74
5	Gibbs	503	5	44.43	66.7	8.84	3.11
6	Gibbs	205	0.5	45.23	64.6	8.70	3.46
7	Minnelusa	506	0.5	45.07	64.4	8.64	3.89
8	Canadian	513	0.5	44.83	66.7	8.92	3.66
				Quartz			
9	Gibbs	496	0.5	47.02	61.3	8.73	1.64
10	Minnelusa	510	0.5	46.42	62.9	8.85	1.66
11	Canadian	507	0.5	46.40	62.3	8.76	1.69
				Dolomite			
12	Gibbs	513	0.5	41.71	68.9	8.75	1.65

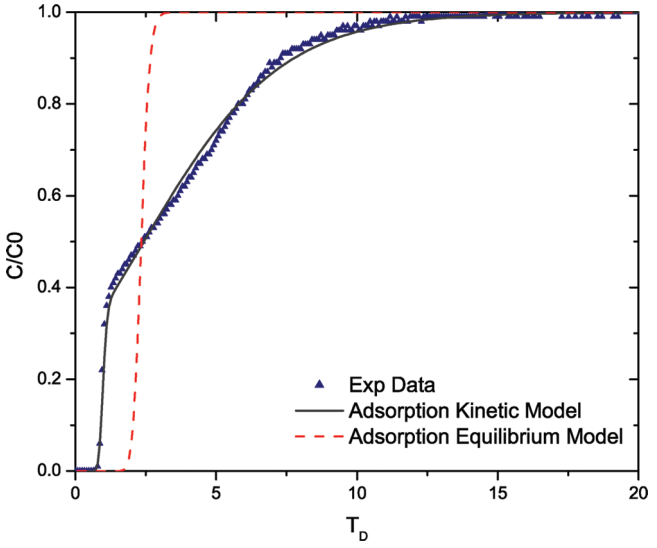

Figure 5. Kinetic adsorption model versus equilibrium adsorption model.

calculations on the measured concentration curves, are provided. To verify whether adsorption is rate-controlled or governed by equilibrium, two independent numerical models, as mentioned in the Modeling section, were prepared and used to find optimized adsorption parameters for each case. Figure 5 shows optimum results for these two models with Gibbs asphaltenes on calcite (experiment 2 in Table 3). Clearly, asphaltene adsorption in porous media is governed by kinetics rather than equilibrium under the experimental conditions of the tests. Thus, the adsorption kinetics model is used to model the rest of the experimental data by optimizing three parameters Γ_m, k_a, and k_d (see Table 4).

On the basis of these optimized parameters, the adsorbed amounts were calculated versus the injected pore volumes and the plateau values predicted by the model are listed in Table 4. There are two adsorption amounts for each experiment reported in this study. The ones tabulated in Table 3 were calculated by material balance from concentration curves and are identified in this work by the subscript "exp". The other set, reported in Table 4, was predicted by our model and is identified by the subscript "model". The effects of flow rate, asphaltene concentration and type, and mineral type are investigated in the following subsections.

Table 4. Kinetic Parameters of Asphaltene Adsorption on Minerals

test	asphaltene	Γ_m (mg/m^2)	k_a (mL mg^{-1} s^{-1})	k_d (s^{-1})	Γ_{model} (mg/m^2)
			Calcite		
1	Gibbs	3.77	8.19×10^{-5}	2.69×10^{-6}	3.54
2	Gibbs	3.77	3.51×10^{-4}	7.44×10^{-6}	3.61
3	Gibbs	3.77	1.02×10^{-3}	6.50×10^{-5}	3.34
4	Gibbs	3.77	1.60×10^{-3}	2.31×10^{-4}	2.94
5	Gibbs	3.77	3.23×10^{-3}	3.35×10^{-4}	3.12
6	Gibbs	3.77	3.51×10^{-4}	7.44×10^{-6}	3.41
7	Minnelusa	5.05	3.58×10^{-4}	5.05×10^{-5}	3.95
8	Canadian	5.02	4.50×10^{-4}	9.53×10^{-5}	3.55
			Quartz		
9	Gibbs	4.66	1.22×10^{-3}	1.14×10^{-3}	1.61
10	Minnelusa	3.66	1.14×10^{-3}	8.00×10^{-4}	1.54
11	Canadian	4.40	1.14×10^{-3}	1.02×10^{-3}	1.59
			Dolomite		
12	Gibbs	4.34	2.13×10^{-4}	1.85×10^{-4}	1.61

Effect of Flow Rate. To study the effect of flow rate on adsorption kinetics, five different flow rates were selected to provide interstitial velocities in the range of 0.05−2.2 cm/min. All of these experiments were conducted with calcite mineral and Gibbs asphaltene solution at a concentration of 500 mg/L (experiments 1−5 in Table 3). The concentration breakthrough curves and model results are shown in Figure 6a, and the modeled adsorbed amounts are presented in Figure 6b. The latter was obtained by adjusting the adsorption and desorption coefficients. Figure 7 shows the total adsorbed amount calculated from material balance at different flow rates. The adsorption amounts at two flow rates (0.5 and 2.5 mL/min) have been measured 3 times to estimate the range of errors. We find that the error in this case does not exceed 7%. Figure 7 indicates a slight decrease in the adsorbed amount with an increasing flow rate.

Researchers provide different explanations in the literature for the effect of flow rate on adsorption. For instance, shear effects, residence time, and zone isolation in the pore space at higher flow rates have been reported in the past.[29,35−37] Our continuum-scale model, however, does not allow for an investigation of the relative impact of various pore-scale phenomena that may be responsible for the

(35) Brusseau, M. *J. Contam. Hydrol.* **1992**, *9*, 353–368.
(36) Haggerty, R.; Harvey, C.; von Schwerin, C.; Meigs, L. *Water Resour. Res.* **2004**, *40*, 1–13.
(37) Ramirez, W.; Shuler, P.; Friedman, F. *SPE J.* **1980**, *20*, 430–438.

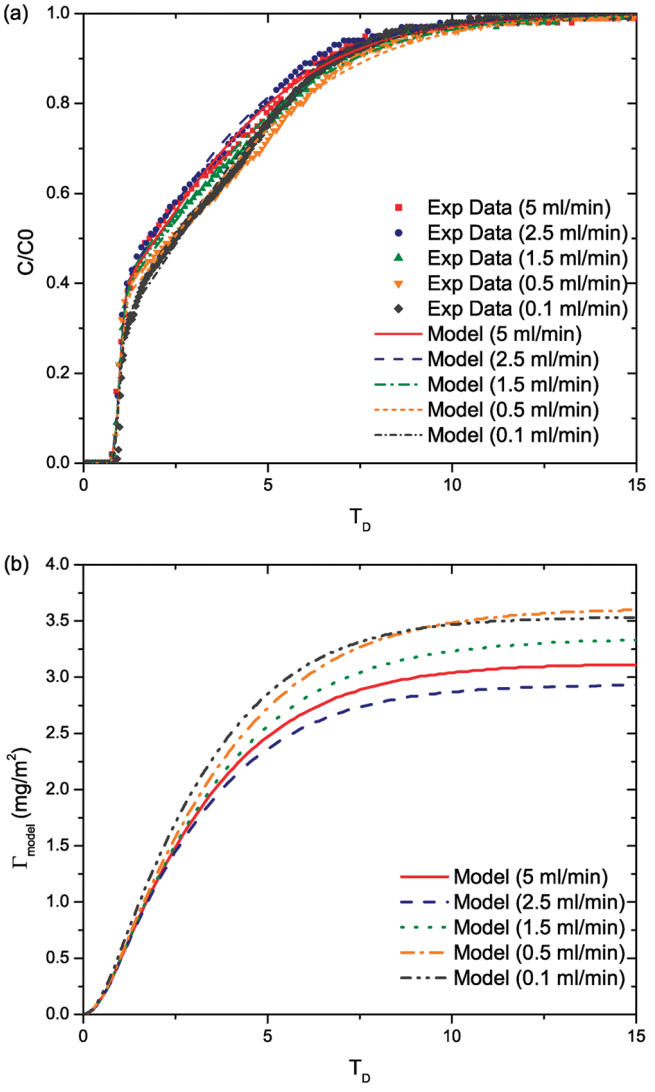

Figure 6. Effect of flow rate on the adsorption of Gibbs asphaltenes on calcite.

observed behavior. Therefore, the adsorption and desorption coefficients in our model act as sink/source parameters. To study the physics responsible for various effects seen here, one would need to use physically-based pore-scale models. Examples of these models include pore-scale network modeling[38] and direct pore-level modeling techniques, such as lattice Boltzmann and moving particle semi-implicit methods.[39,40] Application of these modeling techniques to simulate adsorptive solute transport at the pore level in disordered porous media, however, is beyond the scope of this study.

To investigate the effect of different kinetic parameters on adsorption kinetics in a systematic manner, the hydrodynamic state of the system was kept constant. We used a constant flow rate of 0.5 mL/min for the rest of the experiments.

Effect of Asphaltene Concentration. The effect of the asphaltene concentration is studied with 500 and 200 mg/L Gibbs asphaltenes on calcite (see experiments 2 and 6 in Table 3). Asphaltene molecules tend to form nanoaggregates

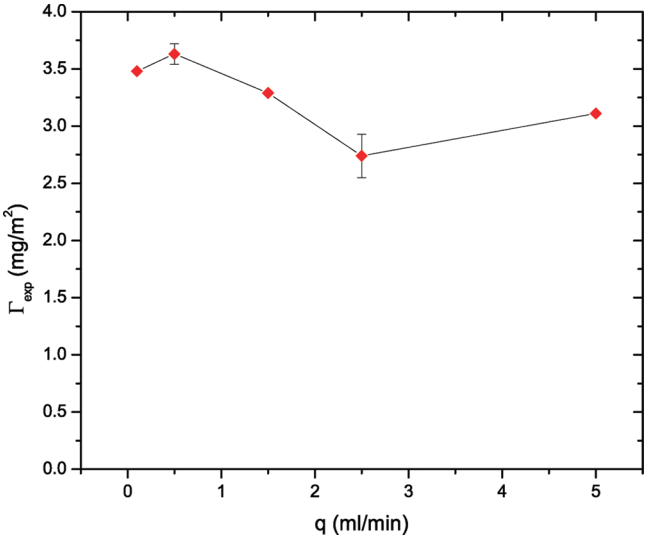

Figure 7. Effect of flow rate on adsorption amount of Gibbs asphaltenes on calcite.

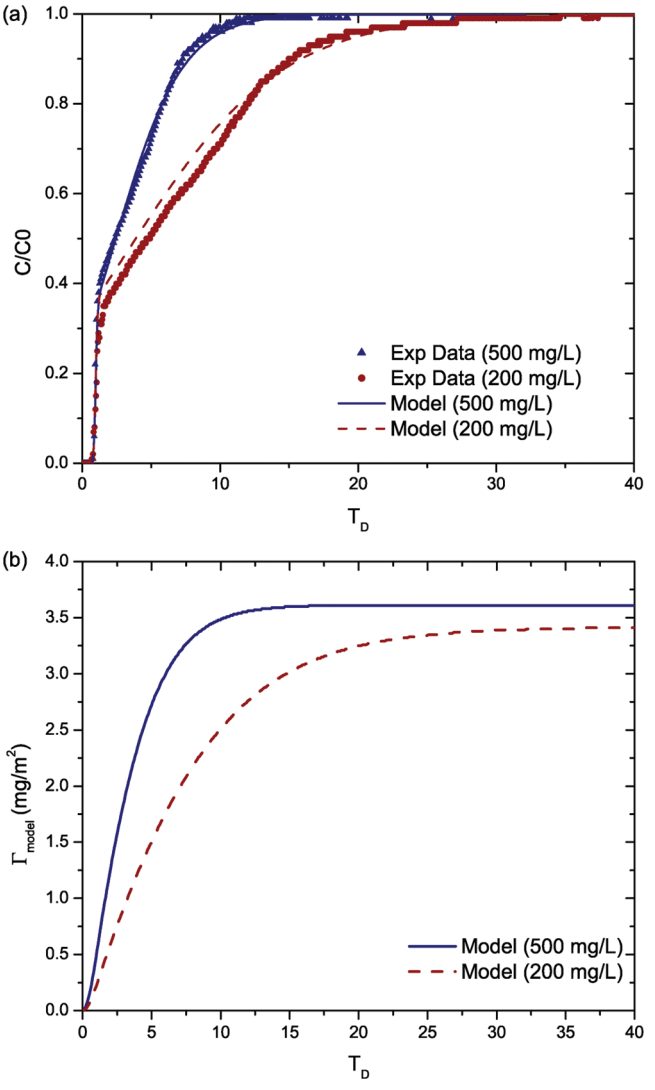

Figure 8. Effect of Gibbs asphaltene concentration on adsorption on calcite.

in the concentration range of 100−5000 mg/L. At this concentration range, the size of nanoaggregates remains

(38) Piri, M.; Blunt, M. J. *Phys. Rev. E: Stat., Nonlinear, Soft Matter Phys.* **2005**, *71*, No. 26301.
(39) Ovaysi, S.; Piri, M. *J. Comput. Phys.* **2010**, *229*, 7456–7476.
(40) Zhang, X.; Lv, M. *J. Hydrol.* **2009**, *371*, 42–52.

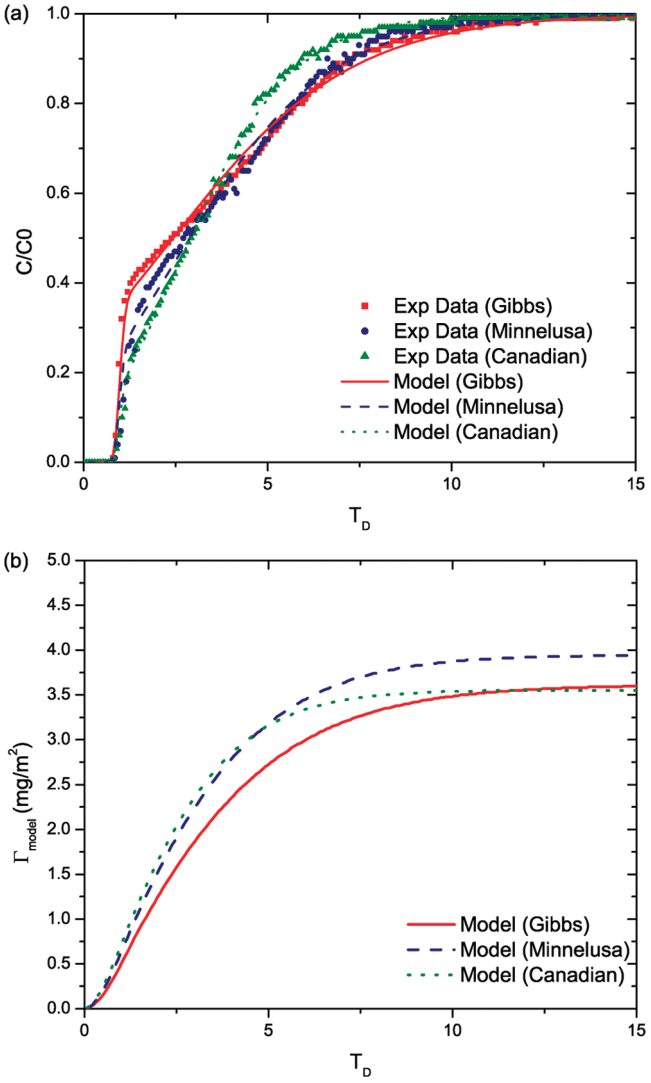

Figure 9. Effect of asphaltene type on adsorption on calcite.

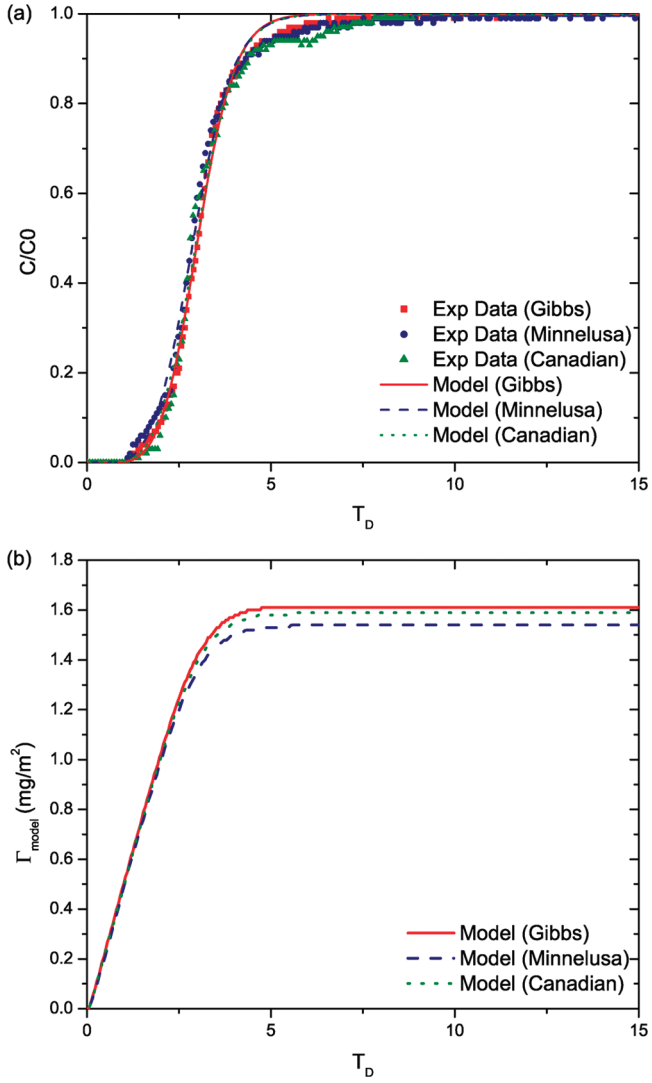

Figure 10. Effect of asphaltene type on adsorption on quartz.

almost constant.[41−44] Figure 8 shows the normalized concentration and adsorption amounts versus injected pore volumes at 200 and 500 mg/L asphaltenes in toluene. The early breakthrough in the concentration curves is the same for both concentrations; however, it takes longer for asphaltenes to reach the injection concentration at 200 mg/L compared to 500 mg/L. As expected, the adsorbed amount at 200 mg/L asphaltenes is smaller than that at 500 mg/L. To further check the validity of the model, the parameters were only optimized for the case of 500 mg/L and are listed in Table 4. Because the TAAD states that the adsorption parameters are concentration-independent and the aggregation state of asphaltene is not expected to vary much in this range of concentration, the same parameters were used to predict the lower concentration breakthrough curve. The modeling results for these two experiments are presented in Figure 8, which show good agreement with the experimental data.

Effect of Asphaltene Type. Figures 9 and 10 illustrate the concentration and adsorption profiles of the three asphaltenes on calcite and quartz, respectively. The concentration profiles for all asphaltenes are very similar on quartz, suggesting that asphaltene type has little influence on the adsorption, in line with previous work under static conditions.[11] On the other hand, Minnelusa asphaltenes adsorb more on calcite than other asphaltenes (see Figure 9). An attempt was made to establish relations between adsorption parameters and asphaltene elemental composition, size, and crude oil acid and base numbers and ratios listed in Table 1. No correlation could be found between these values and adsorption parameters. It appears that the asphaltene type does not have a considerable effect on adsorption, in agreement with the literature.[11]

Effect of Mineral Type. The concentration breakthrough and adsorption profiles for Gibbs asphaltenes and three different minerals (quartz, calcite, and dolomite) are shown in Figure 11. The adsorption plateau is reached faster on quartz than on calcite and dolomite. After 10 pore volumes, the adsorbed amount (Γ) on quartz and dolomite is about the same and is equal to 1.5 mg/m^2. On the other hand,

(41) Goual, L. *Energy Fuels* **2009**, *23*, 2090–2094.
(42) Akbarzadeh, K.; Hammami, A.; Kharrat, A.; Zhang, D.; Allenson, S.; Creek, J.; Kabir, S.; Jamaluddin, A.; Marshall, A.; Rodgers, R.; Mullins, O.; Solbakken, T. *Oilfield Rev.* **2007**, 22–43.
(43) Zeng, H.; Song, Y.-Q.; Johnson, D. L.; Mullins, O. C. *Energy Fuels* **2009**, *23*, 1201–1208.
(44) Freed, D.; Lisitza, N. V.; Song, Y.-Q.; Sen, P. N. Molecular composition and dynamics of oils from diffusion measurements. In *Asphaltenes, Heavy Oils and Petroleomics*; Mullins, O. C., Sheu, E. Y., Hammami, A., Marshall, A. G., Eds.; Springer: New York, 2007; pp 279−296.

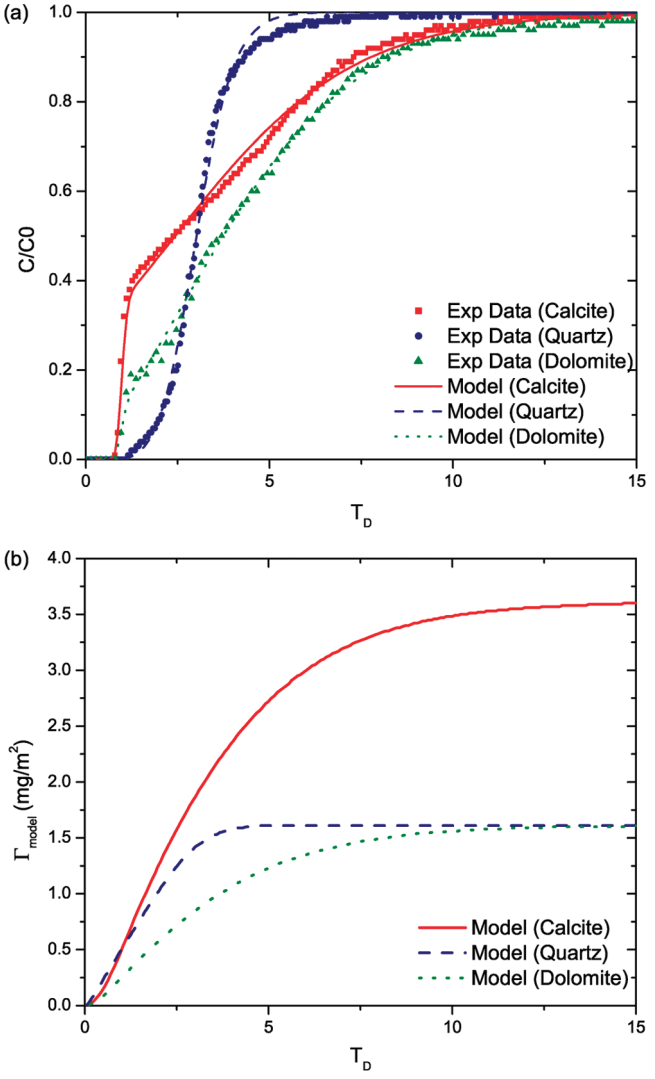

Figure 11. Effect of mineral type on the adsorption of 500 ppm Gibbs asphaltenes.

adsorption is higher on calcite (more than twice the amount adsorbed on quartz and dolomite). Assuming an asphaltene density of 1000 kg/m^3, the thickness of the adsorbed films on minerals is in the range of 1.6−3.9 nm and is comparable to the diameters of asphaltene nanoaggregates estimated from electrical conductivity[41] and spectroscopic studies.[45] These results indicate monolayer adsorption of nanoaggregates. Monolayer adsorption of asphaltenes on quartz or silica has been reported in the past under dynamic conditions,[16] as well as static conditions.[5,11,13,19,45−56]

The differences in adsorption on various minerals cannot be explained by the rock physical properties, such as cumulative pore volume and pore diameter, listed in Table 2, as previously proposed.[18] Furthermore, physical properties, such as mineral shape, may not affect adsorption.[11] It has been shown that calcite mineral is more reactive than quartz in aqueous solution, resulting in more adsorption. However, in low dielectric solvents, such as toluene, explaining the adsorption on various minerals is more challenging because of the lack of experimental studies in the literature. Further studies need to be performed on the chemistry of surfaces in organic solvents and their effects on the microscopic interactions between asphaltene nanoaggregates and minerals.

Conclusions

The adsorption of asphaltenes in porous media is successfully measured under dynamic flow conditions. A numerical convection−dispersion−adsorption model is developed to predict asphaltene adsorption. A comparison of model results with experimental data indicates that the adsorption process is rate-controlled (kinetics) rather than instantaneous (equilibrium). The adsorption kinetics is well described by the TAAD theory. Application of this theory to the model makes it possible to predict different shapes of the measured concentration breakthrough curves. The model can also predict the effect of the asphaltene concentration on adsorption using the same concentration-independent parameters. Asphaltenes show higher adsorption on calcite, while quartz and dolomite have the same adsorption amounts. Nevertheless, we find that asphaltene nanoaggregates form monolayers on all of the minerals. The composition and properties of asphaltenes and crude oils do not show any direct correlation with adsorption. All of the tests of this study were performed under anhydrous conditions. The presence of water in porous media requires detailed consideration of the effect of water on adsorption. This will be the subject of our future work.

Acknowledgment. The authors thank the School of Energy Resources of the University of Wyoming (UW) for financial support and EnCana and the Enhanced Oil Recovery Institute of UW for providing crude oil samples. We also thank Dr. S. Swapp (UW) for sharing rock-crushing facilities.

Nomenclature

ASPH = asphaltene content of crude oil (wt %)
B/A = ratio of the total base number/total acid number
C = solution concentration (mg/mL)
C_0 = initial concentration of injection fluid (mg/mL)
C_D = dimensionless concentration (C/C_0)
D = dispersion coefficient (cm^2/s)
D_m = molecular or aggregate diffusion coefficient (cm^2/s)
H/C = hydrogen/carbon ratio ((wt % of H/molecular weight of H)/(wt % of C/molecular weight of C))
k_a = adsorption rate constant (mL mg^{-1} s^{-1})
k_d = desorption rate constant (s^{-1})
L = sand pack length (cm)
t = time (s)
T_D = dimensionless time (vt/L)
TAN = total acid number (mg of KOH/g)
TBN = total base number (mg of KOH/g)
x = distance in the linear coordinate (cm)

(45) Simon, S.; Jestin, J.; Palermo, T.; Barre, L. *J. Hydrol.* **2009**, *23*, 306–313.
(46) Pfannkuch, H. *Rev. Inst. Fr. Pet.* **1963**, *18*, 1215–270.
(47) Carberry, J.; Bretton, R. *AIChE J.* **1958**, *4*, 367–375.
(48) Edwards, M.; Richardson, J. *AIChE J.* **1968**, *23*, 109–123.
(49) Blackwell, R.; Ryne, J.; Terry, W. *SPE J.* **1959**, *216*, 1–8.
(50) Rifai, M. N. E.; Kaufman, W. J.; Todd, D. K. Dispersion in laminar flow through porous media. *Research Laboratory Report 93-2*; Sanitary Engineering Research Laboratory, University of California: Berkeley, CA, 1956.
(51) Seymour, J.; Callaghan, P. *AIChE J.* **1997**, *43*, 2096–2111.
(52) Kandhai, D.; Hlushkou, D.; Hoekstra, A.; Sloot, P.; As, H. V.; Tallarek, U. *Phys. Rev. Lett.* **2002**, *88*, 234501-1–234501-4.
(53) Khrapitchev, A.; Callaghan, P. *Phys. Fluids* **2003**, *15*, 2649–2660.
(54) Stohr, M. Ph.D. Thesis, University of Heidelberg, Heidelberg, Germany, 2003.
(55) Mullins, O. *Energy Fuels* **2010**, *24*, 2179–2207.
(56) Lobato, M. D.; Pedrosa, J. M.; Möbius, D.; Lago, S. *Langmuir* **2009**, *25*, 1377–1384.

X_D = dimensionless distance (x/L)
Γ = amount adsorbed (mg of asphaltene/g of rock)
Γ_D = dimensionless adsorption (Γ/Γ_m)
Γ_m = maximum amount adsorbed, monolayer capacity (mg of asphaltene/g of rock)
ΔX_D = dimensionless spatial increment
ΔT_D = dimensionless time step
ν = interstitial velocity (Darcy velocity/ϕ)
ρ_r = rock density (g/mL)
ϕ = porosity in the fraction

Appendix

Equations 1 and 2 of the text in dimensionless forms become

$$N_D\frac{\partial^2 C_D}{\partial {X_D}^2}-\frac{\partial C_D}{\partial X_D}=\frac{\partial C_D}{\partial T_D}+N_A\frac{\partial \Gamma_D}{\partial T_D} \quad \text{(A1)}$$

$$\frac{\partial \Gamma_D}{\partial T_D}=N_\nu C_D(1-\Gamma_D)-N_\nu N_k\Gamma_D \quad \text{(A2)}$$

where

$$N_D=\frac{D}{\nu L}=\frac{1}{Pe} \quad \text{(A3)}$$

$$N_A=\frac{(1-\phi)\rho_r\Gamma_m}{\phi C_0} \quad \text{(A4)}$$

$$N_\nu=\frac{k_a C_0 L}{\nu} \quad \text{(A5)}$$

$$N_k=\frac{k_d}{k_a C_0} \quad \text{(A6)}$$

The four dimensionless groups defined in the equations above are the dispersion group (N_D) or inverse of the Peclet number, adsorption capacity group (N_A), rate group (N_ν), and kinetic group (N_k).

The dimensionless form of eq 5 is

$$N_D\frac{\partial^2 C_D}{\partial {X_D}^2}-\frac{\partial C_D}{\partial X_D}=N_{Ae}\frac{\partial C_D}{\partial T_D} \quad \text{(A7)}$$

where

$$N_{Ae}=1+\frac{(1-\phi)\rho_r\Gamma_m K_L}{\phi(1+K_L C_0 C_D)^2} \quad \text{(A8)}$$

A different combination of initial and boundary conditions are used in the literature to solve the convection−dispersion−adsorption equation. Here, Danckwerts' boundary conditions are applied.[22]

$$C_D-N_D\frac{\partial C_D}{\partial X_D}=1 \quad \text{at } X_D=0 \quad \text{(A9)}$$

$$\frac{\partial C_D}{\partial X_D}=0 \quad \text{at } X_D=1 \quad \text{(A10)}$$

$$C_D=0 \quad \text{at } T_D=0 \quad \text{(A11)}$$

$$\Gamma_D=0 \quad \text{at } T_D=0 \quad \text{(A12)}$$